NeuroImage 253 (2022) 119101

Contents lists available at ScienceDirect

NeuroImage

journal homepage: www.elsevier.com/locate/neuroimage

Individual variability in functional organization of the neonatal brain

M. Fiona Molloy, Zeynep M. Saygin*

Department of Psychology, The Ohio State University, 1835 Neil Avenue, Columbus, OH 43210, United States

ARTICLE INFO

Keywords:
Neonates
fMRI
Connectivity
Development
Resting state

ABSTRACT

The adult brain is organized into distinct functional networks, forming the basis of information processing and determining individual differences in behavior. Is this network organization genetically determined and present at birth? And what is the individual variability in this organization in neonates? Here, we use unsupervised learning to uncover intrinsic functional brain organization using resting-state connectivity from a large cohort of neonates (Developing Human Connectome Project). We identified a set of symmetric, hierarchical, and replicable networks: sensorimotor, visual, default mode, ventral attention, and high-level vision. We quantified individual variability across neonates, and found the most individual variability in the ventral attention networks. Crucially, the variability of these networks was not driven by SNR differences or differences from adult networks (Yeo et al., 2011). Finally, differential gene expression provided a potential explanation for the emergence of these distinct networks and identified potential genes of interest for future developmental and individual variability research. Overall, we found neonatal connectomes (even at the voxel-level) can reveal broad individual-specific information processing units. The presence of individual differences in neonates and the framework for personalized parcellations demonstrated here has the potential to improve prediction of behavior and future outcomes from neonatal and infant brain data.

1. Individual variability in the innate functional organization of the human brain

Elucidating the organization of the brain has been a major objective in neuroscience for many decades. By understanding the arealization of the brain, and how brain areas connect and communicate with one another, neuroscientists hope to better understand information processing and how the brain performs complex mental functions. Early approaches to understanding the human brain relied on postmortem samples and similarities in cell types and myelination were used to distinguish between brain areas. Brodmann's areas (Brodmann, 1909), identified via cytoarchitecture, are still widely used to label and identify brain regions in neuroimaging studies. Advancements in noninvasive neuroimaging brought about newer atlases which are based on differences in structure and tissue composition that can be identified with MRI. As opposed to early approaches which were based on postmortem samples from one or a few individuals, these atlases can be identified *in vivo* and are typically based on structural information from a large group of individuals, thus increasing the applicability of these atlases to the general population.

More recently, resting state fMRI scans (measuring spontaneous brain activity) show that the brain is organized into functional networks that support distinct perceptual and cognitive functions e.g., visual, default, limbic, somatomotor, ventral attention, dorsal attention, and control networks (Yeo et al., 2011). These networks were identified by measuring co-fluctuations of BOLD signal during rest (i.e., functional connectivity to the rest of the brain) and clustering brain regions together based on the similarity of this functional connectivity profile. Numerous studies support these conclusions, identifying similar network structures via functional connectivity in the adult cortex (Choi et al., 2018; Power et al., 2011; Smith et al., 2009) and also in the cerebellum (Buckner et al., 2011). There is evidence that this network organization is heritable (Ge et al., 2017; Glahn et al., 2010) and reveals important individual differences that are predictive of individual variability in behavior for both typical individuals (Kong et al., 2019; Rosenberg et al., 2016) and for mental illness (Buckholtz and Meyer-Lindenberg, 2012; van den Heuvel and Sporns, 2019). The importance of considering individual variability in both brain organization and behavior has demonstrated the need for individual-level parcellations (Bijsterbosch et al., 2020). In adults, there exist numerous individualized approaches of varying resolutions based on functional connectivity (Blumensath et al., 2013; Hacker et al., 2013; Kong et al., 2019; Power et al., 2011), surface-based anatomy (Desikan et al., 2006), or multiple modalities (Glasser et al., 2016). Significant work reviewing and directly comparing the myriad of parcellations has revealed there is no perfect approach, and the ideal parcellation depends on the research question (see Thirion et al., 2014; Eickhoff et al., 2018; Arslan et al., 2018 for comprehensive reviews and comparisons for adults). Because of the previously mentioned importance of individual differences in functional connectivity, some approaches in adults individually tune group-level parcellations while enforcing group-level consistency, e.g. based on comparison to average time series within a parcel (Wang et al., 2015)

* Corresponding author.
E-mail address: saygin.3@osu.edu (Z.M. Saygin).

https://doi.org/10.1016/j.neuroimage.2022.119101.
Received 14 October 2021; Received in revised form 28 February 2022; Accepted 14 March 2022
Available online 15 March 2022.

or region-growing algorithms based on distance/similarity to an exemplar time series (Salehi et al., 2020). But the presence of a structured, heritable functional organization and its link to individual variability in behavior in adults brings us back to a fundamental question in neuroscience and psychology: is the organization of the human brain innate and what individual variability in this organization exists at birth?

The human brain undergoes major changes over the first few years of life, including large overall growth and expansion due to e.g. synaptogenesis and myelination, with certain brain regions developing earlier than others (Gogtay et al., 2004; Kinney et al., 1988; Lebel et al., 2008). And yet humans are born with a rich set of mental faculties, presumably supported by existing neural architecture that is genetically determined prenatally (Dehaene-Lambertz and Spelke, 2015; Price et al., 2006; Takahashi et al., 2012). Infant neuroimaging techniques have flourished over the past few years and there is now evidence that young infants display neural signatures for phonetic representations (Dehaene-Lambertz and Gliga, 2004) and sophisticated visual functions such as face and scene processing identified with fMRI and fNIRs (Deen et al., 2017; Farroni et al., 2013); moreover, recent work shows the distinct connectivity patterns present at birth may determine the location of this high-level visual cortex (Kamps et al., 2020; Li et al., 2020; Saygin et al., 2016).

Previous work using resting-state connectivity during natural sleep in preterm infants suggests large-scale organization is present by the 3rd trimester (Doria et al., 2010). More recent studies examining fetal functional connectivity in utero, now provide evidence that this organization is present prenatally (van den Heuvel et al., 2018), with key features present as early as the 2nd trimester (Thomason et al., 2013; Turk et al., 2019). Numerous studies in infants within the first year of life have identified networks (based on fMRI or diffusion weighted imaging) that closely resemble those found in adults using either independent components analyses (ICA; Doria et al., 2010; Fransson et al., 2007, 2011; Gao et al., 2009; Liu et al., 2008; Smyser et al., 2011) or graph theoretical approaches (Ball et al., 2014; Peng et al., 2020; Shi et al., 2018). Additionally, early brain organization can be disrupted by premature birth and/or early experience (Ball et al., 2014; De Asis-Cruz et al., 2020; Scheinost et al., 2016). Most recently, Eyre et al. (2021) used a group-level ICA approach to define resting state networks (based on 24 full-term neonates from the Developing Human Connectome Project). Regression analyses on the larger set of premature and full-term neonates revealed the effects of gestational age and premature birth on these networks, although the effects of individual differences were not explored. This, in addition to the vast literature on the utility of individualized approaches in adults, emphasize the importance of defining individual network organization in infants.

However, these methods required structural constraints, e.g. a priori regions of interest or spatial contiguity (in graph theoretical approaches) or user-specified components (in ICA, typically based on those found in adults) to define the connectome and/or to constrain the boundaries of networks. We apply no constraints based on location or known adult networks, which allows us to uncover both localized and distributed neonate-specific networks based on neonatal resting state connectivity alone. Additionally, instead of excluding components based on lower intersubject agreement, we quantify within-subject agreement of these networks and identify and quantify networks with high variability across subjects. Crucially, while individual differences have been found to alter underlying networks in adults (Kong et al., 2019), it is unclear if, and to what degree, individual variability in brain networks exists at birth. Consequently, we describe a framework to identify individual networks, in addition to the group-level parcellations. To the best of our knowledge, a fine-grained (i.e., voxel by voxel), whole-brain approach to cluster resting state data into broadscale or distributed networks in a large group of newborns has not yet been attempted. Can we use voxelwise connectivity to delineate the intrinsic network structure of the neonate brain? Are these networks distributed and symmetrical like they are in adults? Are they variable among individuals, and what are the underlying differences in genetic expression that may determine this organization prenatally?

We aim to answer these remaining questions about the functional organization of the brain at birth, both across a large group of neonates and within individual neonates (see Fig. 1 for an overview). We use the voxel-wise resting state data from the Developing Human Connectome Project (dHCP; Hughes et al., 2017; https://www.developingconnectome.org) on 267 term-birth newborns and determine voxel-to-voxel functional connectivity. Following a similar approach as Yeo et al. (2011), these data are then clustered based on k-means clustering, a data-driven unsupervised learning approach. We compare training and independent test set clustering solutions for $k = 2$ to $k = 25$ networks and find the optimal solutions on the whole brain (subcortex and cortex) and separately for the cortex only (for direct comparison to the adult clustering solutions from Yeo et al., 2011). We then evaluate individual variability of the resulting networks on the personalized parcellations in the independent test set. Finally, we explore the possible genetic basis of these networks by matching our networks to the genetic data available from the Allen Human Brain Atlas (AHBA; Hawrylycz et al., 2012) and to those that change throughout development using the BrainSpan Atlas of the Developing Human Brain (Miller et al., 2014).

2. Materials and methods

2.1. Neonate dataset

The neonate data are a part of the Developing Human Connectome Project (dHCP; Hughes et al., 2017), a large-scale study of the structural and functional organization of the developing brain. The second release consists of 505 subjects. Only full-term neonates (born at greater than or equal to 37 gestational weeks) with at least one session of functional data that met the dHCP quality control pipeline were included (342 individuals). dHCP quality control checks spanned acquisition, reconstruction, and structural/ functional pipeline metrics (Fitzgibbon et al., 2020; Makropoulos et al., 2018). The quality assurance measures specific to the functional data included checks to minimize subject motion, maximize signal-to-noise, and maximize mutual information between source and reference images. Further, individual sessions were included if there was no sedation during a session (337 individuals), had radiological scores corresponding to “normal” findings, or findings with unlikely clinical/ analysis effects (293 individuals), and successful registration to the group template (missing less than 10 voxels in registration to the neonate template). Thus, the resulting data used here consists of 267 full term neonates (121 females, 146 males); their resting state data comprises of single 15 min scans during natural sleep. The average age at scan was 1.3 chronological weeks (mean gestational age at scan = 41.10 weeks, see full distributions and further details in the Supplementary Materials and Supplementary Fig. 1).

2.2. Ethics statement

The Developing Human Connectome Project was approved by the UK Health Research Authority (Research Ethics Committee reference number: 14/LO/1169). All infants were recruited and scanned at the Evelina Newborn Imaging centre, St Thomas’ Hospital, London, UK and written parental consent was obtained for each individual in the release.

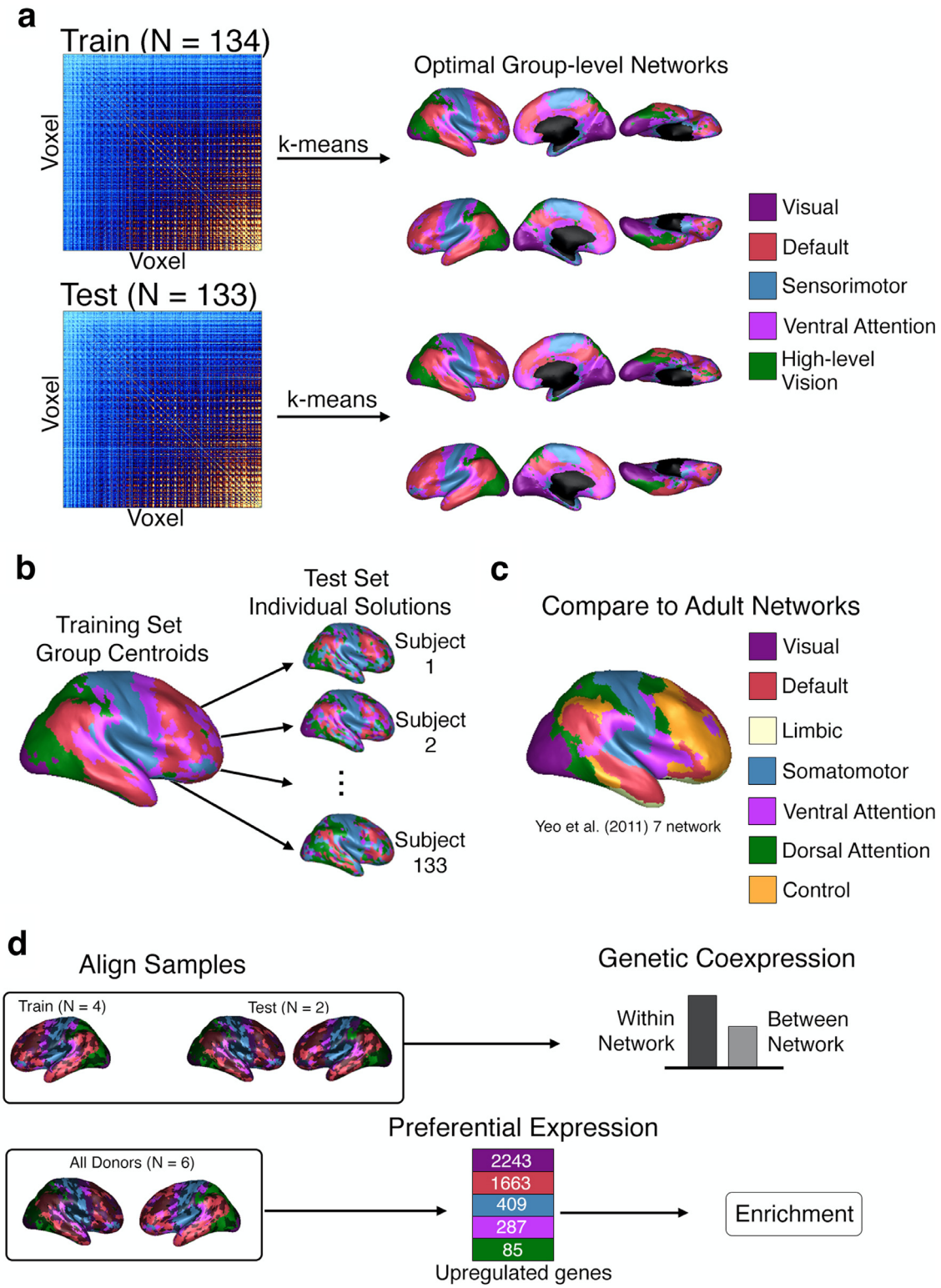

Fig. 1. Overview of Analyses. a. We split neonate data into two randomly defined groups (training and test sets) and calculated voxel-to-voxel functional connectivity (illustrated by the example connectivity matrices). We then calculated clustering solutions (from $k = 2$ to $k = 25$) on the voxel-by-voxel neonate connectome for the training and test sets independently. We identified the optimal networks (optimal k-clusters) based on the best overlap of the train and test solutions. b. To investigate individual variability of these networks, we generated personalized solutions for each individual in the test dataset using the group-level centroids from the training group solutions (5-network solution pictured, with three individual subject results). c. We compared group-level neonate networks to the group-level adult networks from Yeo et al. (2011) and quantified overlap. d. Genetic expression of the networks was explored by aligning samples from the Allen Human Brain Atlas (AHBA) to the 5-network neonate solution. We first split the AHBA samples into training and test groups to explore within and between network genetic expression. We then combined all available data across AHBA donors to find preferentially expressed genes by network.

2.3. Acquisition details

Neonates were scanned using a 3T Philips Achieva (modified R3.2.2 software) with a dedicated neonatal imaging system containing a 32 channel phased head coil (Hughes et al., 2017). High-resolution anatomical images (T2-weighted and inversion recovery T1-weighted multi-slice fast spin-echo images) were acquired with in-plane resolution 0.8 × 0.8mm^2 and 1.6 mm slices overlapped by 0.8 mm (T2w: TE/TR = 156/12,000 ms; T1w: TE/TR/TI = 8.7/4795/1740 ms). Resting-state fMRI data using multiband (MB) 9 × accelerated echo-planar imaging for neonates during natural sleep (sedated infants excluded) were collected (TE/TR = 38/392 ms, voxel size = 2.15 × 2.15 × 2.15 mm^3) for a total of approximately 15 min (2300 vol). Single-band reference scans with bandwidth matched readout, and additional spin-echo acquisitions with both AP/PA fold-over encoding directions were also acquired.

2.4. Preprocessing

The functional data were processed following the dHCP preprocessing pipeline (Fitzgibbon et al., 2020; Makropoulos et al., 2018) and were registered to the 40-week template (Schuh et al., 2018). Additional details summarizing the minimal preprocessing steps are found in the Supplementary Materials and examples of subjects not successfully registered to the group template are shown in Supplementary Fig. 2. Only the cortical gray matter, deep subcortical gray matter, and hippocampus/amygdala voxels were included for connectivity analysis and these were defined according to tissue segmentation masks from the dHCP supplied group atlas (Schuh et al., 2018).

2.5. Defining the connectome

The 267 neonates were then split into a training set of 134 individuals used for tuning the clustering algorithm and a test set of 133 individuals to assess generalizability and replicability (see Supplementary Table 3 for a summary of sex and age in the training and test set). The connectome was defined as the Pearson correlation between each voxel's normalized time series at rest. For the group-average connectomes, individual connectomes were transformed using a Fisher's r to z transform, averaged across the group (either test or train), then transformed back using the inverse Fishers z to r transform. We calculated the connectome for both the whole brain (i.e., cortex and subcortex, resulting in a 23,841 by 23,841 voxel matrix) as well as just the cortex (20,130 by 20,130 voxel matrix) for the training and test sets. We report results from the cortical solutions in the main text and whole-brain solutions in Supplementary Fig. 7.

2.6. Defining networks

We used k-means clustering to define networks on the connectome matrices. K-means clustering is an exploratory, unsupervised learning approach that reveals patterns in the underlying data based on the similarities of features in the observations, which in our case is the similarity of the functional connectivity vectors for each voxel. Similarity was quantified using correlation distance between connectivity vectors; correlation distance captures similarities in connectivity profiles, as opposed to other methods which may capture similarities in the magnitude of connectivity (driven by differences in signal-to-noise ratio, see Supplementary Fig. 4). Further, this metric is equivalent to the distance metric used by Yeo et al. (2011). Five replicates were specified to ameliorate the effect of initial values (the effect of the number of replicates on a resulting solution shown in Supplementary Fig. 6). The resulting networks were color-coded for illustration based roughly on the coloring scheme of the 7-network solution in Yeo et al. (2011)

Because the k-means clustering algorithm is dependent on our choice of the underlying number of clusters, or k, we calculated solutions along a sequence of k clusters ranging from $k = 2$ to 25. These solutions were independently calculated for the training group average connectome and the test group average connectome and evaluated based on fit and stability. The results for all cortical test and train solutions across this entire sequence are shown in Supplementary Figs. 8—12.

An optimal clustering solution should fit the training data well, but also should generalize to the testing data. To fit the data well, a solution should maximize the similarity between voxels in the same cluster and minimize similarity between voxels in different clusters (i.e., maximize separation). We quantified this 'fit' using a metric based on the silhouette coefficient and functional homogeneity (Shi et al., 2018). A silhouette coefficient is calculated for every cluster, k, in each solution. The functional homogeneity silhouette coefficient is defined as

$$SC_k = \frac{a_k - b_k}{max(a_k, b_k)}$$

where a_k is the functional homogeneity within cluster k and $b_k$is the functional homogeneity between voxels in cluster k and other clusters. The within cluster functional homogeneity, a_k is defined as

$$a_k = \frac{\sum_{i,j;i\neq j} corr(v_i, v_j)}{n_k(n_k - 1)}$$

where $n_k$denotes the number of voxels in cluster k, $corr(v_i, v_j)$ is the correlation between voxel i and voxel j (i.e., functional homogeneity of the average training data), and i and j range from 1 to n_k. The between cluster functional homogeneity, b_k, is defined as

$$b_k = \frac{\sum_i \sum_x corr(v_i, v_x)}{n_k(N - n_k)}$$

where $n_k$again denotes the number of voxels in cluster k, $corr(v_i, v_x)$ is the correlation between voxel i in cluster k and voxel x outside of cluster k (i.e., functional homogeneity of the average training data), i ranges from 1 to n_k (including all voxels within cluster k), and x ranges from 1 to $N - n_k$, where N is the total number of voxels (in other words, including all voxels not in cluster k). An ideal solution would maximize a_k and minimize b_k, so an ideal solution would have a larger SC_k. The possible range of SC_k is −1 to 1, where 1 indicates the best possible solution, and −1 indicates the worst possible solution.

Additionally, a solution should generalize to other data well (here, the testing data), to avoid overfitting. A generalizable solution would have a high degree of overlap between the training solution and the testing solution. We use two metrics to generalize overlap: the dice coefficient (Dice, 1945) and the Adjusted Rand Index (ARI; Vinh et al., 2009).

The dice coefficient has been widely used in studies comparing brain parcellations in adults, and we use the same measures used in Arslan et al., (2018). Dice ranges from 0 to 1, where 1 indicates perfect overlap and is defined as

$$DICE_k = \frac{2\,|X_k \cap Y_k|}{|X_k||Y_k|}$$

Where $|X_k \cap Y_k|$ is the number of voxels in both parcel X and parcel Y, $|X_k|$ is the total voxels in X_k, and $|Y_k|$ is the total voxels in Y. Dice is computed for pairs of parcels in two different solutions (here, test and train) with the largest overlap (without replacement), so there is a dice value for each cluster in a given solution. To choose our optimal solution, we use the mean dice.

The ARI is another measure of overlap, but unlike dice, it does not require the pairing of parcels. We use ARI as defined in Arslan et al. (2018) as well. The ARI for two solutions X and Y is

$$ARI(X, Y) = \frac{2(N_{00}N_{11} - N_{01}N_{10})}{(N_{00} + N_{01})(N_{01} + N_{11}) + (N_{00} + N_{10})(N_{10} + N_{11})}$$

where N_{11} indicates the number of pairs of voxels assigned to the same cluster in both solution X and solution Y, N_{00} indicates the number of

pairs of voxels assigned to different clusters in both solution X and solution Y, N_{01} indicates the number of pairs of voxels assigned to different clusters in solution X but the same cluster in solution Y, and N_{10} indicates the number of pairs of voxels assigned to the same cluster in solution X, but different clusters in solution Y.

To define symmetry, we quantify the proportion of voxels with the same network assignment on both hemispheres. In the neonate group template, each voxel in the right hemisphere is projected to the left hemisphere and matched to the nearest left hemispheric voxel. If the left and right voxels have the same network assignment, it is considered symmetric. The overall symmetry measure for a given solution is the proportion of matches for all right hemispheric voxels. Symmetry broken up by network is reported in Supplementary Fig. 15.

2.7. Individual solutions

We used the group centroids calculated from the training set as our prior, and then ran a k-nearest neighbor classifier to assign voxels to the most similar connectivity profile. We did this for every individual in the test set, so we had a total of 133 individual solutions. Between-subject overlap was quantified per voxel by calculating the proportion of individuals with the same network assignment for that voxel (using the independent training set as ground truth for network assignment). Average overlap (using the dice coefficient), and the standard error of the mean across all voxels within each network were also calculated. To calculate within-subject stability of each network, we split the 15-min resting state scan into 5-min segments, then concatenated those sections into three 10-min blocks, calculated the connectome, and calculated the individual solutions. Then, we quantified the within-subject overlap by finding the dice coefficient of overlap across those three solutions. The within- and between-subject overlap for each network was compared using (paired, non-parametric, two-sided) Wilcoxon signed-rank tests. Two additional tests compared the ventral attention network vs. the average overlap of all other networks for within- and between-subject overlaps.

2.8. Comparison to adult networks

The comparison of infant and adult networks was done in (volumetric) adult MNI space (specifically, the FreeSurfer CVS average-35 MNI152 template brain). The neonate group solutions were linearly transformed from the infant template Schuh et al. space to the adult MNI space (Supplementary Figs. 3, 4). Nearest neighbor interpolation was used to transform the parcellation solutions to the adult template space (but not for the initial registration between neonate and adult templates). To account for differences in coverage and fill in gaps from the registrations, the infant solutions were dilated 4 times with a 6 mm kernel, then non-gray matter cortical voxels were removed (defined by tissue masks). The adult 7-network Yeo (liberal mask) solution in MNI space was downloaded from https://surfer.nmr.mgh.harvard.edu/fswiki/CorticalParcellation_Yeo2011. Note that the Yeo et al. solution was computed on the surface, but because of the lack of robust surface methods for neonates, we complete all analyses in the volume space. We calculated the overlap between adult and neonate (the testing solutions for $k = 5$ and $k = 7$) solutions using the dice coefficient as outlined above. Only voxels present in both the MNI images of the Yeo and neonatal solutions were compared.

2.9. Genetic expression by network

Normalized microarray data were obtained from the Allen Human Brain Atlas (AHBA; Hawrylycz et al., 2012). These data include samples of 20,787 genes from six donors. The donors are all adults, and unfortunately, to the best of our knowledge, no whole-brain genetic expression data is currently available with comparable spatial coverage in neonates. These limitations are further addressed in the Discussion. Four donors contained only left hemispheric samples, while the other two contained bihemispheric samples. To explore within/between network differences in genetic expression, the data from the four left hemispheric donors defined the network-specific gene sets, and the data from the bihemispheric donors were used to compare the mean expression of those gene sets within the relevant network and between all other networks (following similar methods as outlined in Anderson et al., 2018 for adult networks). We included data from all six donors to determine each network's preferential genes and enrichment. The microarray data were further preprocessed following steps from Gomez et al. (2019). First, we excluded probes without a gene symbol or Entrez ID. Second, we averaged the expression profiles of all probes targeting the same genes (within an individual). Third, we standardized within each donor.

Before matching the AHBA samples to the neonatal networks, we registered both the AHBA samples and the neonatal networks to FreeSurfer CVS average-35 MNI152 space (details in Supplementary Materials). Additionally, we split the large neonatal networks into smaller sections. First, we separated discontinuous components using nilearn (Pedregosa et al., 2011), separating by hemisphere and excluding regions less than 100 mm^3. Second, very large subregions (more than 1000 voxels) were further divided using a watershed algorithm (Meyer, 1994). Finally, the watershed-defined regions were slightly dilated within the boundaries of the original networks to define the final subregions to which the AHBA samples were matched. Additional matching details including number of subregions matched per individual and network are included in the Supplementary Table 3. Expression values used in the genetic analyses averaged individual samples within the same subregion.

Preferentially expressed genes for each network were compared to the expression of that gene in the average of all other networks using a linear model in the limma package from Ritchie et al. (2015). We accounted for subject-to-subject (across donor) differences using the donor as a blocking variable and the residual donor effects were controlled for using limma's duplicateCorrelation tool. Genes were identified as significantly upregulated only if they passed Bonferroni correction at $q \leq 0.01$ and log2 fold-change (logFC) > 0. Using the samples from the four left-hemispheric donors as the test set, we identified the preferential genes for the five networks. We found a total of 2937 unique preferential genes for the five networks. The gene set for the visual network was the largest (1638 genes), but preferentially expressed genes were identified for all networks (1000 default genes, 103 ventral attention genes, 179 sensorimotor genes, and 12 high-level vision genes). The mean expression for each network's set of genes was calculated for each sample in the test set (remaining two donors), resulting in both within-network and between-network mean expression observations for each sample. We used an ANOVA model (fixed effects for network expression, random effect of donor) to identify if the within network expression was higher than the between network expression. Because these two left out donors contain samples from both hemispheres, the total number of matched observations (465) was comparable to the total number of observations used to define the gene sets (456). Post-hoc tests (one-way ANOVA, random effect of donor) revealed the degree of within- versus between-network differences. We report p-values, F-statistics, effect sizes as indices of partial variance explained (η_p^2), and confidence intervals of the estimated marginal mean difference of between expression – within expression, using the Satterthwaite method. For reporting the preferentially expressed genes and the enrichment analyses, we used data from all six donors, performing an identical limma model analysis as above. Preferentially expressed genes were again defined as those genes with positive logFC that passed Bonferroni correction at $p < 0.01$ for each contrast/network. The gene enrichment analyses were performed with ToppGene Suite (Chen et al., 2009). The enrichment gene sets were defined using the Entrez IDs of the genes identified by each network's preferentially expressed genes. All features were included, with a FDR corrected p-value cutoff of 0.05.

To determine how the genes we identified above change from infancy to adulthood, we conducted additional analyses using the BrainSpan Atlas of the Developing Human Brain (Miller et al., 2014). Specifically, we used the Developmental Transcriptome data which include gene expression data from 16 brain structures including pre-natal (minimum donor age of 8 post-conceptual weeks) and postnatal (maximum donor age of 40 years) samples. First, to identify which genes are significantly changing in levels of expression, differential expression searches were conducted on http://www.brainspan.org/rnaseq/search/index.html. A 2-sample *t*-test for each probe was performed with the null hypothesis that the average expression of samples in the target structures is greater than the average expression of samples in the contrast structures. The two age-groups of interest were limited by the data available in BrainSpan, but included young infants (0–6 months) and young adults (20–40 years). This comprised of samples from two 4-month-old infants and five young adults (age range: 21—37 years, mean: 29.4 years). Searches were completed in both directions (e.g. with young infants as the target and young adults as the contrast, and vice versa) for all cortical structures (excluding the cerebellar cortex), which yielded two lists of overexpressed genes that were changing between infancy and adulthood (developmentally different gene sets). The differential expression tests were one-tailed; thus we only included genes with Benjamini and Hochberg FDR corrected p-values of less than 0.025. Then, for each network, hypergeometric tests were constructed to determine over-representation of the original network gene sets, in the developmentally different gene sets identified from the BrainSpan atlas. The total number of genes compared (i.e., the genes with an Entrez ID tested in both AHBA and the BrainSpan atlas) was 18,955 unique genes.

3. Results

3.1. Optimal solutions

First, we determined neonatal networks underlying high-resolution resting-state connectivity data (Fig. 1a). We calculated voxel-to-voxel connectivity for the training set (134 neonates) and test set (133 neonates) of neonatal resting state data (mean age at scan: 1.31 weeks). These connectomes were clustered based on similarities of voxel-wise connectivity profiles, starting from $k = 2$ to $k = 25$. We then chose the optimal number of networks/ clusters, k, by identifying the solutions that best fit the neonatal data (quantified by the silhouette index, SI) and were reliably reproduced (quantified by the overlap between the independently calculated test and train solutions). The clustering analysis revealed two optimal solutions: $k = 5$ and $k = 8$ (Fig. 2a). These k-solutions produced parcellations that maximized within-network similarity, while minimizing between-network similarity, i.e., these solutions had high SIs (mean: 0.81 for $k = 5$ and 0.90 for $k = 8$). These networks were replicated in the independent test group, indicated by the high overlap between the test and train solutions (mean dice coefficient: 0.89 for $k = 5$ and 0.88 for $k = 8$; Adjusted Rand Index: 0.73 for $k = 5$ and 0.72 for $k = 8$).

The 5-network optimal solutions for the training and test sets are shown in Fig. 2b. Despite the lack of structural or spatial constraints, network components were spatially continuous and symmetric. Approximately 80% of the voxels were symmetric (i.e., had the same network assignment in the corresponding voxel across hemispheres): 80.31% for the training solution and 80.63% for the test solution. The networks corresponding to the visual and sensorimotor networks (purple, green, and blue) were quite spatially localized. Interestingly, these networks were the first to be differentiated at lower k values and were further subdivided as k increased. At $k = 2$, the visual and sensorimotor networks formed one network separated from the rest of the cortex. With $k = 3$, the visual and sensorimotor networks separated into distinct networks. With $k = 4$ and 5 (optimal solution), the visual network split into low-level visual and high-level visual clusters; higher k solutions (including $k = 8$, the other optimal solution, discussed below) revealed a further split of the visual network into anterior/posterior components. The hierarchical emergence of networks is described in more detail (Supplementary Materials) and illustrated in Supplementary Figs. 13 and 14 and Supplementary Movie 1.

For the optimal cluster solution of $k = 5$, the blue cluster, which we refer to as the sensorimotor network, covers the somatosensory cortex, the motor cortex, and parts of the medial temporal lobe. Two of the clusters span the visual cortex. The purple cluster includes much of the occipital cortex and is therefore named the (early) visual network. The other visual network (green cluster in Fig. 2b) strikingly seems to encompass high-level visual cortex spanning the dorsal and ventral visual streams (including occipital and parietal/temporal cortices) and is therefore referred to as the high-level vision network. The remaining clusters (red and magenta) were more distributed across the brain and were named based on qualitative similarities to adult networks (Yeo et al., 2011). The default network (red cluster in Fig. 2b) contains frontal, superior temporal, and superior/parietal regions. Finally, the ventral attention network (magenta cluster in Fig. 2b) is comprised of the frontal eye fields and cingulate gyrus.

The higher-resolution optimal clustering solution revealed eight distinct networks (Fig. 2c). In line with the aforementioned hierarchical emergence of additional networks, the network borders remained roughly the same as those observed in the 5-network solution, but additional clusters emerged in occipitotemporal and parietal regions. In the same manner as the lower resolution solution, the network components were continuous and symmetric (78.76% matching voxels for the training solution and 80.76% matching voxels for the test solution). The ventral attention and sensorimotor networks were highly preserved between the 5-network and 8-network solutions. The other networks in the 8-network solution further segmented the temporal and occipital lobes. The low-level vision network in the 5-network solution was further split into a medial network (purple, Visual I) and a lateral network (light green, Visual II). An additional temporoparietal network (yellow) was distinguished from the lateral posterior components of the default network. Finally, a temporal network (orange) emerged in a region that consisted of the ventral attention and default network in the 5-network solution.

3.2. Individual differences

How are these optimal networks affected by individual differences in connectivity? To answer this, we found individual solutions for the 133 neonates in the testing set, assigning a network for each voxel (for each individual) based on how well that voxel's connectivity profile fit the group-level 5-network solution of the training group (Fig. 1b, see individual examples in Fig. 3a).

The between-subject agreement was defined as the overlap of network assignment averaged across all 133 subjects for each voxel (Fig. 3b, all optimal solutions in Supplementary Fig. 16). The between-subject overlap varied among voxels (mean = 43%, standard deviation = 20%), showing some voxels with very high between-subject overlap (100% of individuals with the same network classification) and voxels with very low between-subject overlap (0.75% of individuals with the same network classification). We found the highest between-subject overlap in the sensorimotor network, which coincides with similar findings in adults (Kong et al., 2019). Moderate between-subject agreement was found in the medial components of the visual network, and in the parietal component of the default network. The network with the lowest between-subject overlap was the ventral attention network. These voxel-wise results were corroborated using the dice coefficient per network (Fig. 3c) showing a similar order of individual variability as the voxel-wise results, with the highest between-subject overlap for sensorimotor areas (mean dice = 0.54 ± 0.0085), and lowest for the ventral attention network (mean dice = 0.23 ± 0.0086). To ensure low overlap was not a result of noise or signal-to-noise ratio differences across the brain, we

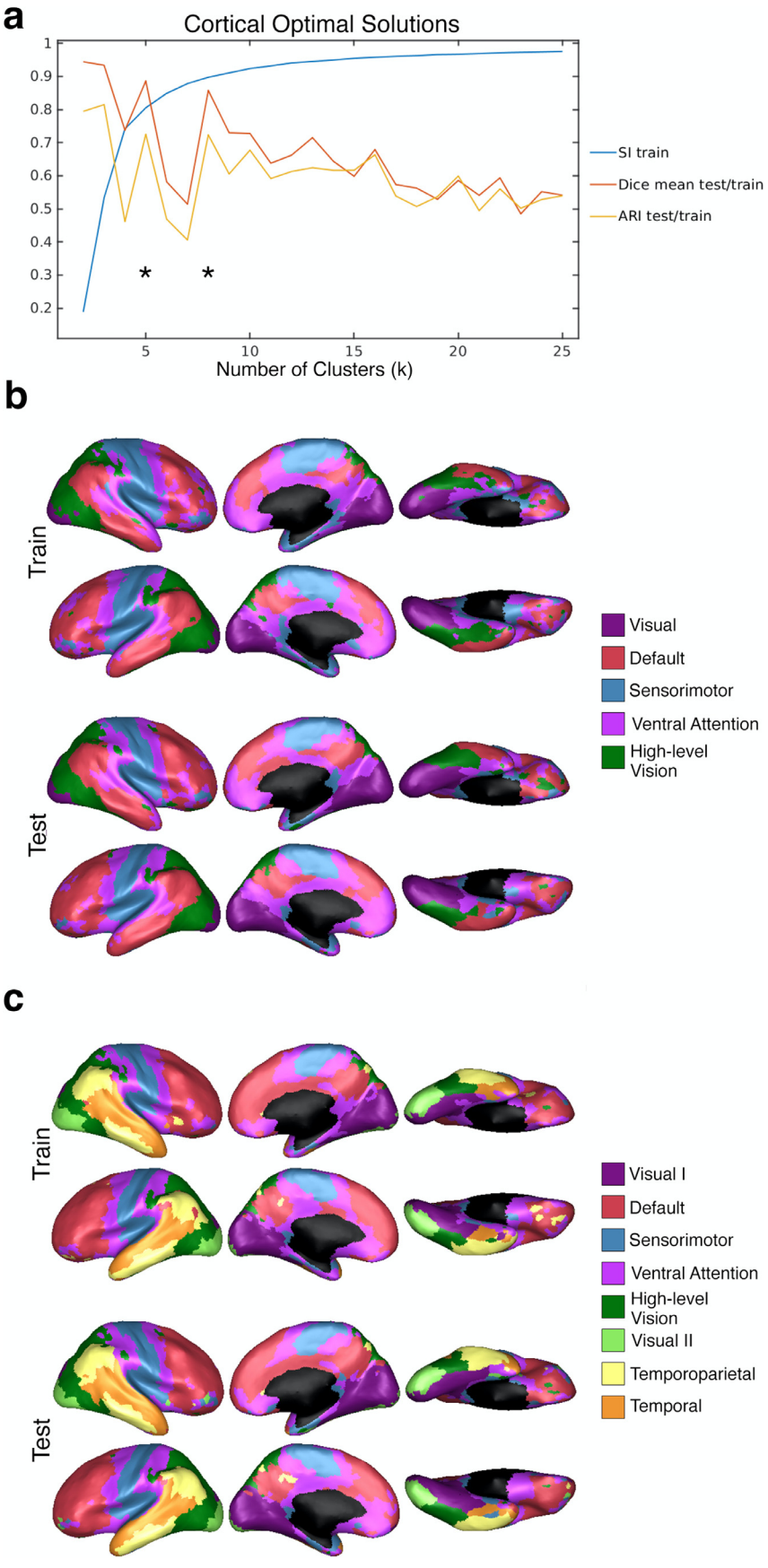

Fig. 2. Optimal Cortical Solutions. a. Quantitative evaluations (y-axis) of clustering solutions for each of the k-clusters (x-axis). The blue line shows the Silhouette Index (SI) for clustering in the training set (essentially the fit of the clustering solutions to the underlying connectivity data). The red and yellow lines show the overlap of the training and test set solutions quantified by the dice coefficient (red line) and Adjusted Rand Index (ARI; yellow line). b. Optimal $k = 5$ solution for the training and test sets. c. Optimal $k = 8$ solution for the training and test sets. b and c illustrate the hemispheric symmetry of the solutions and similarity of the solutions between training and test sets.

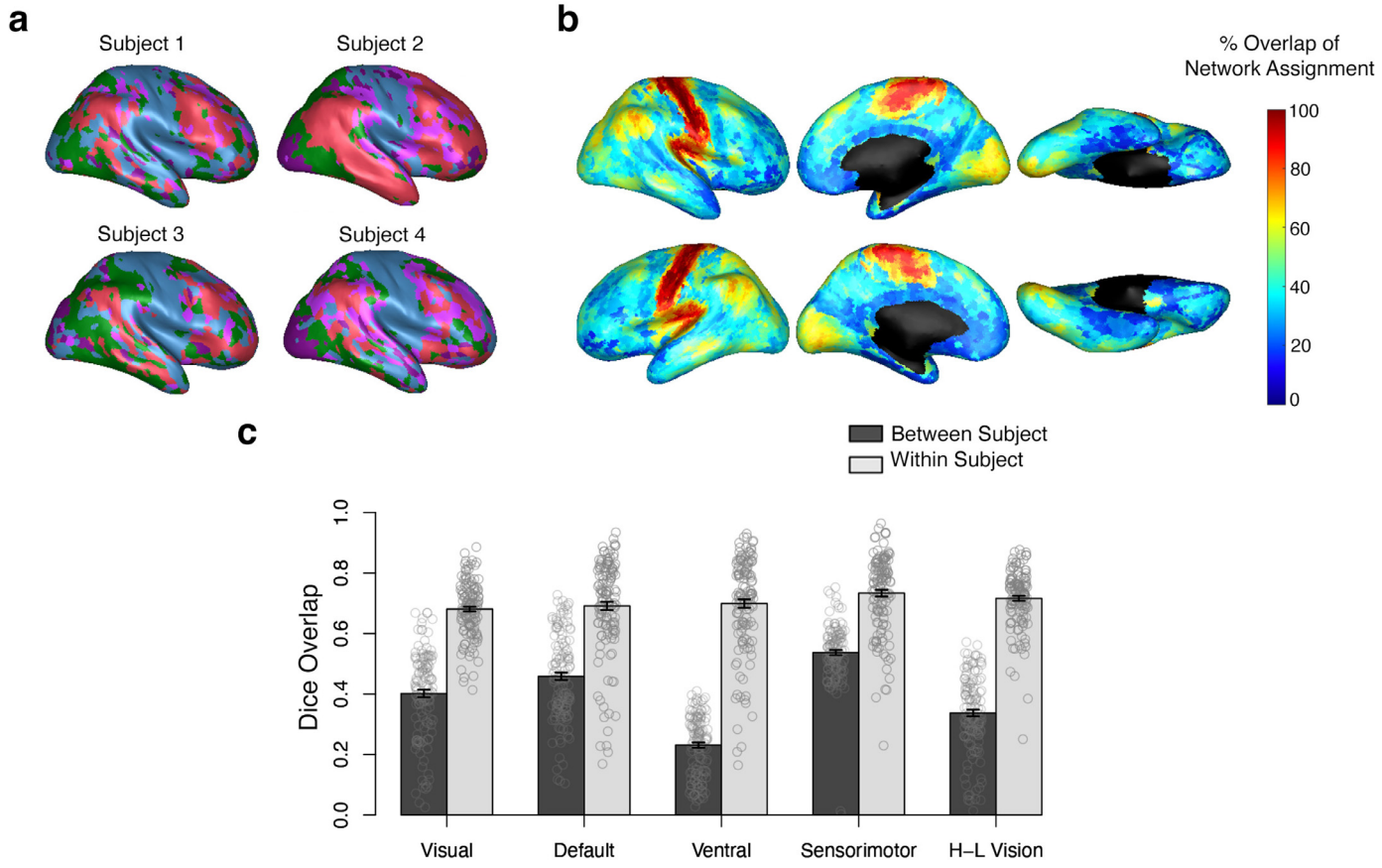

Fig. 3. Individual Differences in the 5-network Solutions. a. Example individual solutions for four randomly selected neonates. b. Voxel-wise between-subject proportion of overlap for the 5 networks. Voxels in warmer colors depict a higher proportion of individuals who were assigned to the same network. c. Within-subject overlap (mean: dark bars, individuals: open circles) and between-subject overlap (mean: light bars, individuals: open circles) for all voxels within a network. For all networks, the within-subject overlap is significantly higher than the between-subject overlap (paired Wilcoxon signed-rank $p \leq 0.001$ for all networks). The error bars indicate ± 1 standard error of the mean.

calculated within-subject overlap of network solutions by splitting up each neonate's connectivity data into three 10-min resting state time-series and generating three independent connectome solutions per subject. Fig. 3b shows the mean overlap within each network for between-subject overlap, and within-subject overlap. Across all networks, within-subject similarity was higher than the between-subject similarity (non-parametric paired two-sided Wilcoxon signed rank $p \leq 0.001$ for each network, Cohen's $d > 0.80$ for each network, Supplementary Table 2). Moreover, individual variability found in the ventral attention network does not appear to be driven by higher noise within that network, as the within-subject variability does not differ from other networks (two-sided Wilcoxon signed rank $V = 4819$, $p = 0.41$, $d = -0.012$, 95% CI [−0.019,0.042] for within-subject overlap in ventral attention versus all others, compared to $V = 41$, $p = 3.7 \times 10^{-23}$, $d = -1.2$, 95% CI [−0.22,−0.18] for between-subject overlap in ventral attention versus all others).

3.3. Comparison to adults

We next directly compared the group-level optimal network solutions between neonates and those previously identified in adults. Fig. 4a shows the 5-network neonate solution found here and the adult 7-network solution (Yeo et al., 2011). Many of the networks identified in neonates resemble those in the adults including (as labeled in the Yeo atlas): visual, default, somatomotor, ventral attention, and dorsal attention networks. However, there were no neonate networks matching the control or limbic adult networks (see Supplementary Fig. 17 for a quantitative comparison). This suggests that regions in the limbic and control networks lack discrete connectivity patterns in neonates such that they cannot be easily separated from the rest of the cortex.

However, it is plausible these networks could emerge if the total number of networks in neonates is assumed to be the same as the total number of networks in adults. To test this, we next compared the 7-network solution for neonates to the 7-network solution in adults (Fig. 4c). The highest overlapping networks were the sensorimotor network (dice = 0.75) and the default network (dice = 0.62). Interestingly, the dice coefficients for the adult control and limbic networks remain very close to zero (control = 0.000302 and limbic = 0.00985). Thus, even at higher k-solutions, there were no neonatal networks that resembled the adult control and limbic networks. Instead, the two vision-related networks in the neonate 5-network solution (high-level vision and vision) were further split, yielding four visual networks in the 7-network solution for neonates (see also Supplementary Fig. 14 for illustration of hierarchy of networks with increasing k).

3.4. Genetic expression

The results so far suggest prenatal mechanisms determine cortical connectivity such that these distinct functional networks are already present at birth, even in the absence of rich postnatal sensory experiences. What are the potential genetic differences driving these networks? Previous work revealed distinct genetic expression profiles for cortical networks in adults (Anderson et al., 2018; Richiardi et al., 2015). We followed similar analyses as Anderson et al. (2018) using tissue samples from six donors available through the Allan Human Brain Atlas (AHBA) to explore the correspondence of the neonatal networks

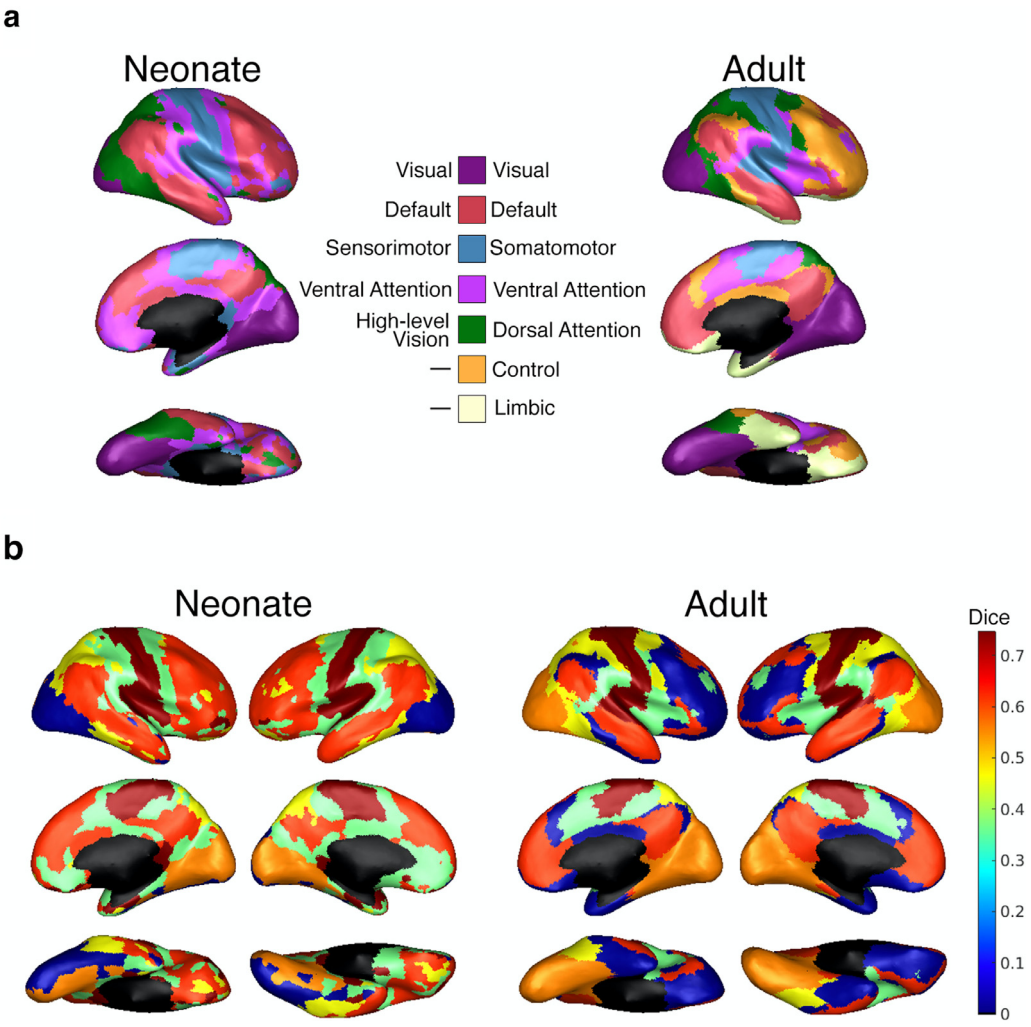

Fig. 4. Comparison to Adult Networks. a. Lowest optimal solution for neonates (k = 5 networks) and for adults (k = 7 networks, from Yeo et al., 2011). b. Dice overlap between matched pairs of neonate (k = 7) and adult (k = 7) networks. Warmer colors indicate a network is more similar between neonates and adults. The results are plotted onto the neonate networks (left) and the adult networks (right).

and genetic expression (Fig. 1d). The first analysis determines how well gene sets preferentially expressed in one network account for genetic variability within that network compared to others. The second analysis explores the degree to which these network-specific gene sets change throughout development.

In the first analysis, to characterize differential expression by network, we assigned samples to each network from: i. four donors to define network specific gene sets and ii. two donors to independently test how well those gene sets account for within- and between-network genetic expression (Fig. 5a). Preferentially expressed gene sets for each network included genes with a significant (Bonferroni-corrected $q \leq 0.01$) positive log2 fold-change expression in that network versus the average of all others. We used the samples in the independent donors (remaining two donors) to compare within- and between-network expression of these gene sets (Fig. 5b). Overall, within-network expression (mean = 0.33±0.023) was higher than between-network expression (mean = 0.12±0.011; F(1, 1873)=123.99, $p < 2.2 \times 10^{-16}$, η_p^2=0.06, 95% CI [−0.24,−0.17]). There was a significant difference within- vs. between-network expression for genes in the visual (F(1, 373.28)=102.92, $p = 2.2 \times 10^{-16}$, η_p^2=0.22, 99% CI [−0.58,−0.35]), default (F(1, 373.11)=34.18,$p = 1.1 \times 10^{-8}$, η_p^2=0.08, 99% CI [−0.27,−0.10]), ventral (F(1, 372.62)=13.41, $p = 2.9 \times 10^{-4}$, η_p^2=0.03, 99% CI [−0.30,−0.052]), high-level vision networks (F(1, 373.26) = 32.81, $p = 2.1 \times 10^{-8}$, η_p^2=0.08, 99% CI [−0.47,−0.18]), and a trend for the sensorimotor network (F(1, 3.518)=5.24, p = 0.093, η_p^2=0.60, 99% CI [−0.30,0.11]).

In the enrichment analysis, to maximize the number of samples, we used data from all six donors (Fig. 5c) to define the preferential gene sets (Fig. 5d). While the total number of genes per network increased due to an increase in power, the relative size of each gene set was similar to the gene sets previously defined. The most significantly upregulated genes (FDR < 0.01 for each contrast of network vs. all other networks) were found in the visual network, with 2243 total preferentially expressed genes. These findings were similar to those in adults which showed the most preferentially expressed genes in the adult limbic and visual networks (Anderson et al., 2018). The default network had the second most preferentially expressed genes with 1663 genes. In decreasing order, the number of upregulated genes for the remaining networks were: 409 in the ventral attention network, 287 in the sensorimotor network, and 85 in the high-level vision network. Full lists of significantly upregulated genes and functional enrichment (e.g., potential biological and cellular functions and related diseases) are found in the Supplementary Data and Supplementary Tables 3–7.

Each network's candidate gene set was initially based on data from the AHBA because of the large number of samples and high-resolution brain coverage. However, the underlying samples are all from adults, so how stable are these network gene sets throughout development? To answer this question, we conducted a follow-up analysis using the

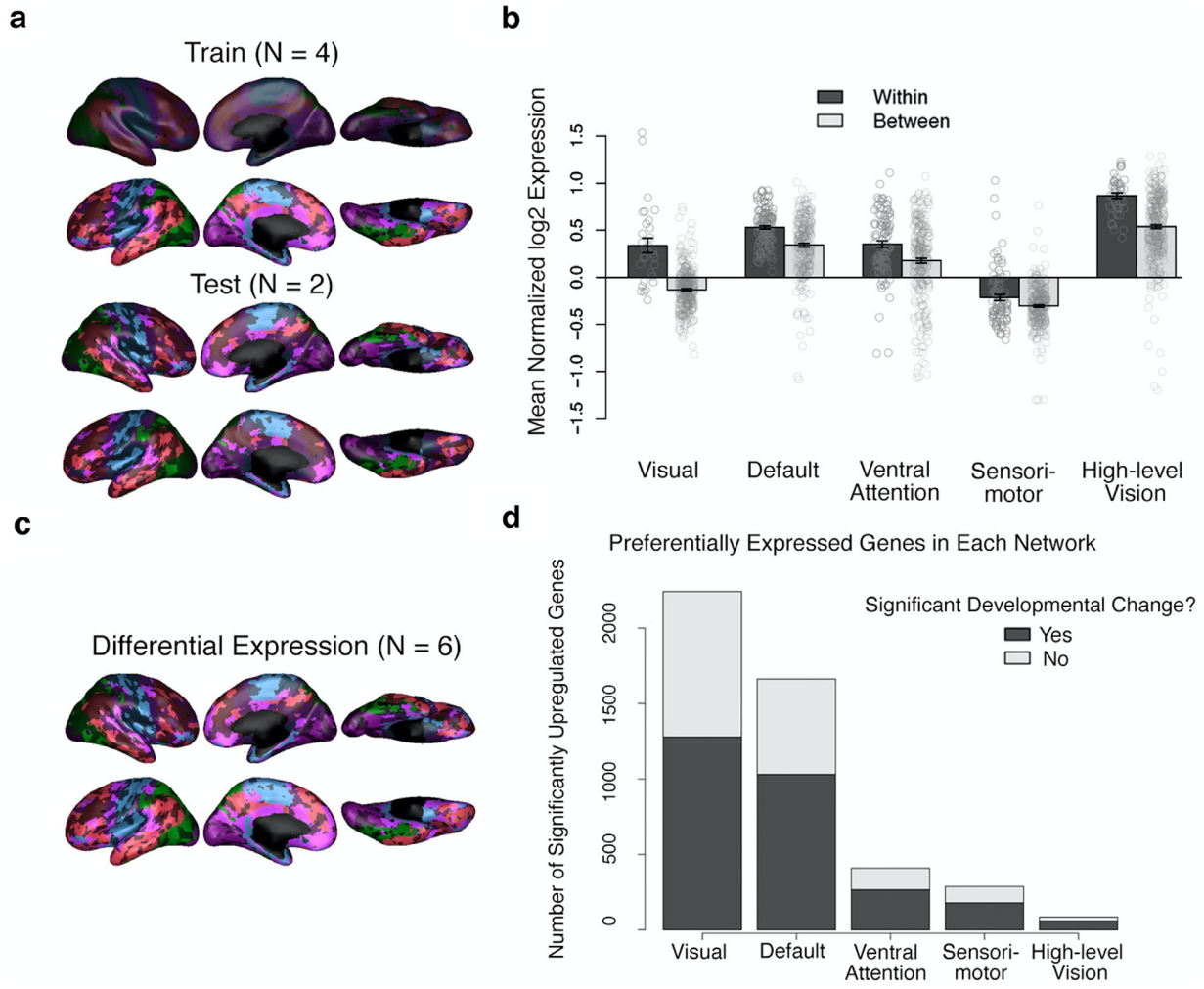

Fig. 5. Genetic Expression by Network. a. Location of samples matched from the four left-hemispheric donors (top: used to define the network-specific gene sets) and the two bihemispheric donors (bottom: used to test the genetic expression within and between each network). Black-shaded regions indicate there was no matching sample/ no available donor data for that region. b. Genetic expression of each network's preferential genes (identified from the four training donors) for within-network samples (mean: dark bars, observations: open circles) and between-network samples (mean: light bars, observations: open circles) for the two test donors. The error bars show ± 1 standard error of the mean. c. Location of samples matched to data from all available donors. d. Number of significant preferentially expressed genes (Bonferroni corrected p-value < 0.01) for each network versus the average of all other networks. The shaded regions of the bar denote the genes that change throughout development while the unshaded portions denote the genes that are not significantly different throughout development or are probed only in the adult samples.

BrainSpan Atlas of the Developing Human Brain (Miller et al., 2014). This BrainSpan atlas has small sample size and sparse coverage of brain tissue, but despite these limitations, may offer important insight into the stability of these gene sets across development. We used the Developmental Transcriptome which includes gene expression data from 16 cortical structures across prenatal to adult samples. Based on the ages of the dHCP neonates and AHBA donors, we focused on cortical changes across two age-groups of interest: young infants (0–6 months) and young adults (20–40 years). Across the brain, we identified 9932 genes that significantly differed between infants and adults. As expected, we found that genes changed across development for all networks (all $p < 0.05$). The number of significantly changing genes per network are shown in the shaded bars in Fig. 5d. Hypergeometric tests were conducted to determine overrepresentation of the network-specific genes with the genes significantly changing from infancy to adulthood, as identified from the BrainSpan data. Significant changes (from smallest to largest p-values) were: default ($p = 1.50 \times 10^{-9}$) < ventral attention ($p = 4.04 \times 10^{-6}$) < high-level vision ($p = 8.85 \times 10^{-4}$) < visual ($p = 1.42 \times 10^{-3}$) < sensorimotor ($p = 2.22 \times 10^{-2}$). Thus, the ventral attention and default mode network-specific genes appear to change most between the two age groups. In other words, the association networks had the highest overexpression of developmentally changing genes.

4. Discussion

In adults, brain regions fluctuate with one another at rest, organizing the brain into distinct functional networks that support complex mental functions and vary across individuals. We investigated this spontaneous, intrinsic brain activity in a large cohort of newborns scanned within one week of life and used an entirely data-driven approach to cluster these dense voxelwise connectomes into discrete networks on both group and individual levels.

We discovered that even in the neonate brain, connectivity profiles of neighboring voxels are distinct enough to be separable into different networks. Much like those observed in adults, neonates had both local and distributed networks that emerged hierarchically, were symmetrical, and, crucially, were replicated across two independent groups. This is also consistent with recent approaches in neonates using a smaller subset of the dHCP and an ICA approach to define resting state networks (Eyre et al., 2021). Quantitative comparisons to the adult net-

works revealed that sensorimotor and visual networks were adult-like, but that frontoparietal cortices were less dissociable into separate networks in neonates, suggesting immature connectivity profiles in these regions. While some previous work is consistent with these findings (Fransson et al., 2007; Gao et al., 2015, but see Doria et al., 2010) our approach provides binary parcellations rather than weighted resting state networks (e.g. through ICA). Critically, because our approach does not rely on assumptions of adult-like network presence in infants, but instead chooses network solutions based on fit and replicability, we found that specifically it is the (frontomedial) control and limbic networks that are immature in neonates. The optimal 5-network solution for neonates did not show these regions as discrete networks. Even when given the opportunity to split into different networks (i.e., at higher clustering solutions), the neonate connectome simply further split up the visual cortices (especially the ventral pathways) rather than splitting these frontomedial cortices into separate networks.

Instead, we discovered the following hierarchy of networks with increasing k-solutions: the first network to dissociate from the rest of the brain was the sensorimotor network which included visual and somatomotor cortex. Next, the visual cortex (both early and late visual cortex) split off from the sensorimotor network, followed by further divisions of visual cortex into a low and high-level visual cortex in the 5-network solution. The high-level visual network clearly displays a split into dorsal and ventral streams, suggesting that perhaps the connectivity of these regions is already set up to perform these high-level functions, which is in line with recent work in infants and neonates (Cabral et al., 2020; Kamps et al., 2020; Li et al., 2020). The visual and high-level visual clusters then further split into anterior/posterior and medial/lateral divisions. High-level visual cortices have gradients or divisions of functional organization based on a combination of retinotopy, animacy, size and other factors in human adults and other animals (Arcaro and Livingstone, 2017; Gomez et al., 2019; Grill-Spector and Weiner, 2014; Hasson et al., 2002; Konkle and Caramazza, 2013; Malach et al., 2002); these gradients and divisions closely mimic the connectivity-based divisions that we observe here in human neonates. The present results suggest that the proto-organization of category-selective visual cortex is not merely retinotopic (not simply clustered within early visual cortex), but rather that it may have important domain-specific connections that are already present at birth.

In contrast to the visual cortices, adult-like control and limbic networks in the frontal cortices were not observed in neonates. The higher clustering solutions that were stable and replicable mainly yielded further subdivision of visual networks. Neonate connectivity did not dissociate between default mode cortex and other frontoparietal and medial frontal cortex. Because of this, neonates had a single large frontoparietal network (here, called the default mode network due to the high overlap with the Yeo default mode network), which subsumed the area where the control network is in adults. Additionally, the optimal neonate solutions did not have any network which resembled the limbic network in Yeo et al. (2011). The neonatal regions in the proximity of the adult limbic network consisted of multiple, distinct connectivity signatures and were thus part of four different distributed networks (all neonatal networks except for visual). These differences from the adult networks were not attributable to individual variability or within-subject instability. Overall, these results show that domain-specific regions, such as categorical visual areas, have a distinct connectivity signature that separates them from adjacent cortices even at birth, whereas cortices involved in more domain-general processing, such as the cognitive control network, do not have distinct connectivity patterns and may need relevant experience to entrain and preferentially fluctuate with, e.g., other nodes in the control network.

We then identified individual subject solutions, in addition to the group-level network solutions, demonstrating the utility of this approach in exploring individual variability. We found particular networks, such as the ventral attention network, were more variable across individuals despite high within-subject consistency. The sensorimotor and visual areas were the most consistent across individuals, and the ventral attention network had the most between-subject differences, replicating patterns previously found in adults (Kong et al., 2019). This variability is likely not a result of noise, as within-subject network variability was high and consistent across networks. These inter-individual differences may be attributed to differences in developmental trajectory. Previous work exploring group-level networks and cortical growth found that these functional networks and brain regions have different developmental trajectories over the first two years, with sensorimotor and visual areas maturing earlier than attention or control networks (Dehaene-Lambertz and Spelke, 2015; Gao et al., 2015; Gogtay et al., 2004). The degree of individual differences observed here also follows this succession, suggesting individual differences may converge with development and maturation. Alternatively, this individual variability in the ventral attention network may indicate some stable source of individual differences, as the ventral attention network has also been found to exhibit the highest inter-individual variability in adults compared to other networks (Kong et al., 2019). Kong et al. also found that this variability was not due to confounding factors (e.g., network size), but it did relate to individual differences in behavior. Future work can use the connectivity-centroids identified here and apply them to individual subject connectomes (as we do here) to delineate individual solutions for participants and track them across time to better understand the divergence or convergence of individual variability across development and its relationship to individual variation in behavior.

Finally, we showed the dissociability of these networks can be at least partially explained by the underlying genetic expression in these cortices. This result suggests the proto-organization of cortex as outlined here, may be determined in large part by early genetic instruction. This conclusion is corroborated by recent work linking structural organization at birth to regional differences in fetal genetic patterns (Ball et al., 2020). Ball et al. explored a similar subset of full-term individuals from the dHCP, but instead focused on structural changes, using the structural MRI and diffusion weighted imaging data. The major structural differences were captured by a component separating primary motor and sensory cortex from association cortices, and fetal genetic patterns mirrored this gradient. Our analyses are consistent with these results: based on functional connectivity (and corroborated by genetic expression), we found a sensorimotor network that was separable from association cortices (namely default and ventral attention). While Ball et al. did not specifically investigate occipital structures and corresponding genetic patterns, they did find a second structural component that separated the visual network from all others. Similarly, we found that a large number of genes were specific to the resting-state cluster corresponding to the visual network. These and other studies underscore the differential genetic basis and development of the hierarchical organization of the visual cortices (e.g Gomez et al., 2019). The visual network is clearly a candidate for future work exploring the relationship between function, structure, and the role of experience and genetics.

The genetic enrichment analyses revealed significant gene sets that are related to nervous system development, and diseases with deficits related to the known function of the network (e.g., preferentially expressed genes in the sensorimotor network were related to cerebral palsy). The differential genetic expression analyses corroborated similar analysis of the adult networks (Anderson et al., 2018). We also observed higher within- than between-network genetic expression and identified similar magnitudes of upregulated genes (Anderson et al., 2018). These similarities suggest the neonate networks are also dissociable based on underlying differences in genetic expression. Critically, while we found all networks showed developmental changes in gene expression, the networks with frontoparietal components showed the most robust developmental changes in gene expression; these networks were also the ones that differed the most from the adult atlas, and that showed the most individual variation across neonates. Conversely, the visual and sensorimotor networks had the lowest overexpression of genes that changed

throughout development, which is consistent with earlier structural maturity of these networks (Gilmore et al., 2018).

Future work is necessary to determine the developmental trajectory of these networks (including possible genetic changes and relationship to future behavior) and to address methodological limitations. First, only full-term infants were analyzed here. Identifying networks in preterm neonates, or in longitudinal resting state sessions throughout the first few years of life, could clarify the timeline of the development of these networks and could ascertain if individual differences within networks converge or diverge with development. Second, the networks we have identified are putative functional networks with nomenclature based on topography or overlap with adult networks. Longitudinal studies could identify the relationship between these networks and various mental functions as they manifest, e.g., measured via behavioral measures, such as language and literary skills (Yu et al., 2020), and/or neural measures, such as task-based fMRI (Saygin et al., 2016). Third, the majority of our genetic analyses, including the definition of the network-specific gene sets, are based on adult tissue samples, and are strictly exploratory. We identified some major developmental changes between infancy and adulthood, but future analyses can explore the developmental progression, including the influence of the perinatal transition, of the various preferentially expressed gene sets identified here. Additionally, as genetic variation affects cortex structure in adults and neonates, further work may reveal if individual variability in functional networks relates to genetic variability.

Finally, some methodological differences could affect the comparison with adult networks. The neonate connectome was computed based on voxel-to-voxel connectivity unlike the Yeo et al. adult connectomes which were computed on a slightly lower resolution supravoxel space. We believe this is actually a strength of the current method, especially because the neonate brain is much smaller than the adult brain. Additionally, while there are differences in the unsupervised clustering algorithms used, the Yeo networks remain relatively stable across parcellation methodologies and datasets (Yeo et al., 2014). The k-means algorithm was chosen here due to its similarity to the approach from Yeo et al. (2011) and it is appropriate for lower resolution solutions (Thirion et al., 2014). However, by definition, k-means yields a binary parcellation (e.g., each voxel can only be assigned to one network). Future analyses could incorporate probabilistic networks (e.g. fuzzy clustering) or a measure of confidence in network assignment. In addition, our nearest-neighbor approach to defining these networks on a new individual's brain preserves individual variation and differs from previous group-informed individualization approaches in adults by comparing a new individual's connectivity profiles to an independent group solution, instead of a non-independent group solution (Salehi et al., 2020; Wang et al., 2015). Specifically, our approach has no spatial constraints (thus allowing for discontinuous networks) and our original group-based centroids are not modified to accommodate a new individual (ensuring true independence of the individual solutions). Emphasizing spatial continuity (Salehi et al., 2020) or incorporating multiple iterations to change network centroids (Wang et al., 2015) could provide additional constraints on the individualized solution, depending on the goal of the researcher, e.g. if interested in functionally homogenous subunits, as opposed to high-level networks (Arslan et al., 2018). Further, our analyses were performed based on currently available, state-of-the-art image processing methods and standard preprocessing techniques. However, the methods available for infants and neonates are not as advanced as the methods currently available for adults. These differences complicate adult and neonatal comparisons, as the transformation between adult and neonatal space is nontrivial. We attempt to ameliorate these differences throughout our analyses and perform the main analyses in neonatal image space, but future improvements of developmental neuroimaging methods will likely improve the results and inferences drawn from the current study.

We provide a way for researchers to apply our clustering solutions to their individual subject connectivity data such that they can obtain subject-specific networks for their data (i.e. by identifying which cluster best matches each voxel's connectivity pattern; available here: https://github.com/SayginLab/neonate_molloy). These subject-specific networks address a growing need for more personalized models in predicting future outcomes, as discussed in Chen et al. (2021). We also provide the atlas for each k clustering solution so that the clusters can simply be overlaid on subject or group data for e.g. seeds and targets for connectivity analyses or as regions of interest for fMRI analyses.

5. Conclusions

Overall, we identified underlying neonatal networks from resting state data that can be identified on an individual level and may be explained by genetic data. Individual differences were present in some networks, such as ventral attention, while others, including sensorimotor were more homogeneous across individuals. Further, some networks, including the control and limbic networks did not appear to be present, or distinguishable based on connectivity, in neonates. These findings indicate some proto-organization at birth, while also highlighting the necessity of experience for full adult-like organization.

Data availability

The neuroimaging data used in this study are available as part of the publicly available Developing Human Connectome Project (dHCP; https://www.developingconnectome.org). The genetic data are from the publicly available Allen Human Brain Atlas (AHBA; http://human.brain-map.org/static/download) and BrainSpan Atlas of the Developing Human Brain (http://brainspan.org/static/download.html). Resulting neonate parcellations and full genetic expression results can be found at https://github.com/SayginLab/neonate_molloy.

Code availability

Analyses were completed using MATLAB R2020a (The MathWorks Inc., Natick, USA) and R version 4.0.3 (2020–10–10). MATLAB code to calculate individual parcellations will be publicly available at https://github.com/SayginLab/neonate_molloy. All code is available from the authors upon request.

Declaration of Competing Interest

None.

Credit authorship contribution statement

M. Fiona Molloy: Conceptualization, Data curation, Formal analysis, Investigation, Methodology, Writing – original draft. **Zeynep M. Saygin:** Conceptualization, Formal analysis, Funding acquisition, Investigation, Methodology, Supervision, Writing – review & editing.

Acknowledgements

Data were provided by the Developing Human Connectome Project, KCL-Imperial-Oxford Consortium funded by the European Research Council under the European Union Seventh Framework Programme (FP/2007–2013) / ERC Grant Agreement no. [319456]. We are grateful to the families who generously supported this work. Analyses were completed using the Ohio Supercomputer Center (https://www.osc.edu). This research was partly funded by the Alfred P. Sloan Foundation (to Z.M.S), Ohio State's Chronic Brain Injury Program (to Z.M.S), and Ohio State University's College of Arts and Sciences (to Z.M.S. and M.F.M.)

Supplementary materials

Supplementary material associated with this article can be found, in the online version, at doi:10.1016/j.neuroimage.2022.119101.

References

Anderson, K.M., Krienen, F.M., Choi, E.Y., Reinen, J.M., Yeo, B.T.T., Holmes, A.J., 2018. Gene expression links functional networks across cortex and striatum. Nat. Commun. 9 (1), 1428. doi:10.1038/s41467-018-03811-x.

Arcaro, M.J., Livingstone, M.S., 2017. A hierarchical, retinotopic proto-organization of the primate visual system at birth. Elife 6, e26196. doi:10.7554/eLife.26196.

Arslan, S., Ktena, S.I., Makropoulos, A., Robinson, E.C., Rueckert, D., Parisot, S., 2018. Human brain mapping: a systematic comparison of parcellation methods for the human cerebral cortex. Neuroimage 170, 5–30. doi:10.1016/j.neuroimage.2017.04.014.

Ball, G., Aljabar, P., Zebari, S., Tusor, N., Arichi, T., Merchant, N., Robinson, E.C., Ogundipe, E., Rueckert, D., Edwards, A.D., Counsell, S.J., 2014. Rich-club organization of the newborn human brain. Proc. Natl. Acad. Sci. 111 (20), 7456–7461. doi:10.1073/pnas.1324118111.

Ball, G., Seidlitz, J., O'Muircheartaigh, J., Dimitrova, R., Fenchel, D., Makropoulos, A., Christiaens, D., Schuh, A., Passerat-Palmbach, J., Hutter, J., Cordero-Grande, L., Hughes, E., Price, A., Hajnal, J.V., Rueckert, D., Robinson, E.C., Edwards, A.D., 2020. Cortical morphology at birth reflects spatiotemporal patterns of gene expression in the fetal human brain. PLoS Biol. 18 (11), e3000976. doi:10.1371/journal.pbio.3000976.

Bijsterbosch, J., Harrison, S.J., Jbabdi, S., Woolrich, M., Beckmann, C., Smith, S., Duff, E.P., 2020. Challenges and future directions for representations of functional brain organization. Nat. Neurosci. 1–12. doi:10.1038/s41593-020-00726-z.

Blumensath, T., Jbabdi, S., Glasser, M.F., Van Essen, D.C., Ugurbil, K., Behrens, T.E.J., Smith, S.M., 2013. Spatially constrained hierarchical parcellation of the brain with resting-state fMRI. Neuroimage 76, 313–324. doi:10.1016/j.neuroimage.2013.03.024.

Brodmann, K., 1909. Vergleichende Lokalisationslehre der Grosshirnrinde in Ihren Prinzipien dargestellt Auf Grund des Zellenbaues. Barth.

Buckholtz, J.W., Meyer-Lindenberg, A., 2012. Psychopathology and the human connectome: toward a transdiagnostic model of risk for mental illness. Neuron 74 (6), 990–1004. doi:10.1016/j.neuron.2012.06.002.

Buckner, R.L., Krienen, F.M., Castellanos, A., Diaz, J.C., Yeo, B.T.T., 2011. The organization of the human cerebellum estimated by intrinsic functional connectivity. J. Neurophysiol. 106 (5), 2322–2345. doi:10.1152/jn.00339.2011.

Cabral, L., Zubiaurre, L., Wild, C., Linke, A., & Cusack, R. (2020). Category-selective visual regions have distinctive signatures of connectivity in neonates. BioRxiv, 675421. 10.1101/675421

Chen, J., Bardes, E.E., Aronow, B.J., Jegga, A.G., 2009. ToppGene Suite for gene list enrichment analysis and candidate gene prioritization. Nucleic Acids Res. 37, W305–W311. doi:10.1093/nar/gkp427, Web Server issue.

Chen, Y., Liu, S., Salzwedel, A., Stephens, R., Cornea, E., Goldman, B.D., Gilmore, J.H., Gao, W., 2021. The subgrouping structure of newborns with heterogenous brain–behavior relationships. Cereb. Cortex 31 (1), 301–311. doi:10.1093/cercor/bhaa226.

Choi, E.Y., Drayna, G.K., Badre, D., 2018. Evidence for a functional hierarchy of association networks. J. Cognit. Neurosci. 30 (5), 722–736. doi:10.1162/jocn_a_01229.

De Asis-Cruz, J., Kapse, K., Basu, S.K., Said, M., Scheinost, D., Murnick, J., Chang, T., du Plessis, A., Limperopoulos, C., 2020. Functional brain connectivity in ex utero premature infants compared to in utero fetuses. Neuroimage 219, 117043. doi:10.1016/j.neuroimage.2020.117043.

Deen, B., Richardson, H., Dilks, D.D., Takahashi, A., Keil, B., Wald, L.L., Kanwisher, N., Saxe, R., 2017. Organization of high-level visual cortex in human infants. Nat. Commun. 8. doi:10.1038/ncomms13995.

Dehaene-Lambertz, G., Gliga, T., 2004. Common neural basis for phoneme processing in infants and adults. J. Cognit. Neurosci. 16 (8), 1375–1387. doi:10.1162/0898929042304714.

Dehaene-Lambertz, G., Spelke, E.S., 2015. The infancy of the human brain. Neuron 88 (1), 93–109. doi:10.1016/j.neuron.2015.09.026.

Desikan, R.S., Ségonne, F., Fischl, B., Quinn, B.T., Dickerson, B.C., Blacker, D., Buckner, R.L., Dale, A.M., Maguire, R.P., Hyman, B.T., Albert, M.S., Killiany, R.J., 2006. An automated labeling system for subdividing the human cerebral cortex on MRI scans into gyral based regions of interest. Neuroimage 31 (3). doi:10.1016/j.neuroimage.2006.01.021.

Dice, L.R., 1945. Measures of the amount of ecologic association between species. Ecology 26 (3), 297–302. doi:10.2307/1932409.

Doria, V., Beckmann, C.F., Arichi, T., Merchant, N., Groppo, M., Turkheimer, F.E., Counsell, S.J., Murgasova, M., Aljabar, P., Nunes, R.G., Larkman, D.J., Rees, G., Edwards, A.D., 2010. Emergence of resting state networks in the preterm human brain. Proc. Natl. Acad. Sci. U. S. A. 107 (46), 20015–20020. doi:10.1073/pnas.1007921107.

Eickhoff, S.B., Yeo, B.T.T., Genon, S., 2018. Imaging-based parcellations of the human brain. Nat. Rev. Neurosci. 19 (11), 672–686. doi:10.1038/s41583-018-0071-7.

Eyre, M., Fitzgibbon, S.P., Ciarrusta, J., Cordero-Grande, L., Price, A.N., Poppe, T., Schuh, A., Hughes, E., O'Keeffe, C., Brandon, J., Cromb, D., Vecchiato, K., Andersson, J., Duff, E.P., Counsell, S.J., Smith, S.M., Rueckert, D., Hajnal, J.V., Arichi, T., …, Edwards, A.D., 2021. The developing human connectome project: typical and disrupted perinatal functional connectivity. Brain 144 (7), 2199–2213. doi:10.1093/brain/awab118.

Farroni, T., Chiarelli, A.M., Lloyd-Fox, S., Massaccesi, S., Merla, A., Di Gangi, V., Mattarello, T., Faraguna, D., Johnson, M.H., 2013. Infant cortex responds to other humans from shortly after birth. Sci. Rep. 3 (1), 2851. doi:10.1038/srep02851.

Fitzgibbon, S.P., Harrison, S.J., Jenkinson, M., Baxter, L., Robinson, E.C., Bastiani, M., Bozek, J., Karolis, V., Cordero Grande, L., Price, A.N., Hughes, E., Makropoulos, A., Passerat-Palmbach, J., Schuh, A., Gao, J., Farahibozorg, S.-R., O'Muircheartaigh, J., Ciarrusta, J., O'Keeffe, C., …, Andersson, J., 2020. The developing Human Connectome Project (dHCP) automated resting-state functional processing framework for newborn infants. Neuroimage 223, 117303. doi:10.1016/j.neuroimage.2020.117303.

Fransson, P., Åden, U., Blennow, M., Lagercrantz, H., 2011. The functional architecture of the infant brain as revealed by resting-state fMRI. Cereb. Cortex 21 (1), 145–154. doi:10.1093/cercor/bhq071.

Fransson, P., Skiöld, B., Horsch, S., Nordell, A., Blennow, M., Lagercrantz, H., Åden, U., 2007. Resting-state networks in the infant brain. Proc. Natl. Acad. Sci. U. S. . 104 (39), 15531–15536. doi:10.1073/pnas.0704380104.

Gao, W., Alcauter, S., Smith, J.K., Gilmore, J., Lin, W., 2015. Development of human brain cortical network architecture during infancy. Brain Struct Funct 220 (2), 1173–1186. doi:10.1007/s00429-014-0710-3.

Gao, W., Zhu, H., Giovanello, K.S., Smith, J.K., Shen, D., Gilmore, J.H., Lin, W., 2009. Evidence on the emergence of the brain's default network from 2-week-old to 2-year-old healthy pediatric subjects. Proc. Natl. Acad. Sci. U. S. A. 106 (16), 6790–6795. doi:10.1073/pnas.0811221106.

Ge, T., Holmes, A.J., Buckner, R.L., Smoller, J.W., Sabuncu, M.R., 2017. Heritability analysis with repeat measurements and its application to resting-state functional connectivity. Proc. Natl. Acad. Sci. 114 (21), 5521–5526.

Gilmore, J.H., Knickmeyer, R.C., Gao, W., 2018. Imaging structural and functional brain development in early childhood. Nat. Rev. Neurosci. 19 (3), 123–137. doi:10.1038/nrn.2018.1.

Glahn, D.C., Winkler, A.M., Kochunov, P., Almasy, L., Duggirala, R., Carless, M.A., Curran, J.C., Olvera, R.L., Laird, A.R., Smith, S.M., Beckmann, C.F., Fox, P.T., Blangero, J., 2010. Genetic control over the resting brain. Proc. Natl. Acad. Sci. 107 (3), 1223–1228. doi:10.1073/pnas.0909969107.

Glasser, M.F., Coalson, T.S., Robinson, E.C., Hacker, C.D., Harwell, J., Yacoub, E., Ugurbil, K., Andersson, J., Beckmann, C.F., Jenkinson, M., Smith, S.M., Van Essen, D.C., 2016. A multi-modal parcellation of human cerebral cortex. Nature 536 (7615), 171–178. doi:10.1038/nature18933.

Gogtay, N., Giedd, J.N., Lusk, L., Hayashi, K.M., Greenstein, D., Vaituzis, A.C., Nugent, T.F., Herman, D.H., Clasen, L.S., Toga, A.W., Rapoport, J.L., Thompson, P.M., 2004. Dynamic mapping of human cortical development during childhood through early adulthood. Proc. Natl. Acad. Sci. U. S. A. 101 (21), 8174–8179. doi:10.1073/pnas.0402680101.

Gomez, J., Zhen, Z., Weiner, K.S., 2019. Human visual cortex is organized along two genetically opposed hierarchical gradients with unique developmental and evolutionary origins. PLoS Biol. 17 (7), e3000362. doi:10.1371/journal.pbio.3000362.

Grill-Spector, K., Weiner, K.S., 2014. The functional architecture of the ventral temporal cortex and its role in categorization. Nat. Rev. Neurosci. 15 (8), 536–548. doi:10.1038/nrn3747.

Hacker, C.D., Laumann, T.O., Szrama, N.P., Baldassarre, A., Snyder, A.Z., Leuthardt, E.C., Corbetta, M., 2013. Resting state network estimation in individual subjects. Neuroimage 82, 616–633. doi:10.1016/j.neuroimage.2013.05.108.

Hasson, U., Levy, I., Behrmann, M., Hendler, T., Malach, R., 2002. Eccentricity bias as an organizing principle for human high-order object areas. Neuron 34 (3), 479–490. doi:10.1016/S0896-6273(02)00662-1.

Hawrylycz, M.J., Lein, E.S., Guillozet-Bongaarts, A.L., Shen, E.H., Ng, L., Miller, J.A., van de Lagemaat, L.N., Smith, K.A., Ebbert, A., Riley, Z.L., Abajian, C., Beckmann, C.F., Bernard, A., Bertagnolli, D., Boe, A.F., Cartagena, P.M., Chakravarty, M.M., Chapin, M., Chong, J., …, Jones, A.R., 2012. An anatomically comprehensive atlas of the adult human brain transcriptome. Nature 489 (7416), 391–399. doi:10.1038/nature11405.

Hughes, E.J., Winchman, T., Padormo, F., Teixeira, R., Wurie, J., Sharma, M., Fox, M., Hutter, J., Cordero-Grande, L., Price, A.N., Allsop, J., Bueno-Conde, J., Tusor, N., Arichi, T., Edwards, A.D., Rutherford, M.A., Counsell, S.J., Hajnal, J.V., 2017. A dedicated neonatal brain imaging system. Magn. Reson. Med. 78 (2), 794–804. doi:10.1002/mrm.26462.

Kamps, F.S., Hendrix, C.L., Brennan, P.A., Dilks, D.D., 2020. Connectivity at the origins of domain specificity in the cortical face and place networks. Proc. Natl. Acad. Sci. 117 (11), 6163–6169. doi:10.1073/pnas.1911359117.

Kinney, H.C., Brody, B.A., Kloman, A.S., Gilles, F.H., 1988. Sequence of central nervous system myelination in human infancy. II. Patterns of myelination in autopsied infants. J. Neuropathol. Exp. Neurol. 47 (3), 217–234. doi:10.1097/00005072-198805000-00003.

Kong, R., Li, J., Orban, C., Sabuncu, M.R., Liu, H., Schaefer, A., Sun, N., Zuo, X.N., Holmes, A.J., Eickhoff, S.B., Yeo, B.T.T., 2019. Spatial topography of individual-specific cortical networks predicts human cognition, personality, and emotion. Cereb. Cortex 29 (6), 2533–2551. doi:10.1093/cercor/bhy123.

Konkle, T., Caramazza, A., 2013. Tripartite organization of the ventral stream by animacy and object size. J. Neurosci. 33 (25), 10235–10242. doi:10.1523/JNEUROSCI.0983-13.2013.

Lebel, C., Walker, L., Leemans, A., Phillips, L., Beaulieu, C., 2008. Microstructural maturation of the human brain from childhood to adulthood. Neuroimage 40 (3), 1044–1055. doi:10.1016/j.neuroimage.2007.12.053.

Li, J., Osher, D.E., Hansen, H.A., Saygin, Z.M., 2020. Innate connectivity patterns drive the development of the visual word form area. Sci. Rep. 10 (1), 1–12. doi:10.1038/s41598-020-75015-7.

Liu, W.C., Flax, J.F., Guise, K.G., Sukul, V., Benasich, A.A., 2008. Functional connectivity of the sensorimotor area in naturally sleeping infants. Brain Res. 1223, 42–49. doi:10.1016/j.brainres.2008.05.054.

Makropoulos, A., Robinson, E.C., Schuh, A., Wright, R., Fitzgibbon, S., Bozek, J., Counsell, S.J., Steinweg, J., Vecchiato, K., Passerat-Palmbach, J., Lenz, G., Mortari, F.,

Tenev, T., Duff, E.P., Bastiani, M., Cordero-Grande, L., Hughes, E., Tusor, N., Tournier, J.-D., …, Rueckert, D., 2018. The developing human connectome project: a minimal processing pipeline for neonatal cortical surface reconstruction. Neuroimage 173, 88–112. doi:10.1016/j.neuroimage.2018.01.054.

Malach, R., Levy, I., Hasson, U., 2002. The topography of high-order human object areas. Trends Cognit. Sci. 6 (4), 176–184. doi:10.1016/s1364-6613(02)01870-3, (Regul. Ed.).

Meyer, F., 1994. Topographic distance and watershed lines. Signal Process. 38 (1), 113–125. doi:10.1016/0165-1684(94)90060-4.

Miller, J.A., Ding, S.L., Sunkin, S.M., Smith, K.A., Ng, L., Szafer, A., Ebbert, A., Riley, Z.L., Royall, J.J., Aiona, K., Arnold, J.M., Bennet, C., Bertagnolli, D., Brouner, K., Butler, S., Caldejon, S., Carey, A., Cuhaciyan, C., Dalley, R.A., …, Lein, E.S., 2014. Transcriptional landscape of the prenatal human brain. Nature 508 (7495), 199–206. doi:10.1038/nature13185.

Pedregosa, F., Varoquaux, G., Gramfort, A., Michel, V., Thirion, B., Grisel, O., Blondel, M., Prettenhofer, P., Weiss, R., Dubourg, V., Vanderplas, J., Passos, A., Cournapeau, D., Brucher, M., Perrot, M., Duchesnay, É., 2011. Scikit-learn: machine learning in python. J. Mach. Learn. Res. 12 (85), 2825–2830.

Peng, Q., Ouyang, M., Wang, J., Yu, Q., Zhao, C., Slinger, M., Li, H., Fan, Y., Hong, B., Huang, H., 2020. Regularized-Ncut: robust and homogeneous functional parcellation of neonate and adult brain networks. Artif. Intell. Med. 106, 101872. doi:10.1016/j.artmed.2020.101872.

Power, J.D., Cohen, A.L., Nelson, S.M., Wig, G.S., Barnes, K.A., Church, J.A., Vogel, A.C., Laumann, T.O., Miezin, F.M., Schlaggar, B.L., Petersen, S.E., 2011. Functional network organization of the human brain. Neuron 72 (4), 665–678. doi:10.1016/j.neuron.2011.09.006.

Price, D.J., Kennedy, H., Dehay, C., Zhou, L., Mercier, M., Jossin, Y., Goffinet, A.M., Tissir, F., Blakey, D., Molnár, Z., 2006. The development of cortical connections. Eur. J. Neurosci. 23 (4), 910–920. doi:10.1111/j.1460-9568.2006.04620.x.

Richiardi, J., Altmann, A., Milazzo, A.-C., Chang, C., Chakravarty, M.M., Banaschewski, T., Barker, G.J., Bokde, A.L.W., Bromberg, U., Büchel, C., Conrod, P., Fauth-Bühler, M., Flor, H., Frouin, V., Gallinat, J., Garavan, H., Gowland, P., Heinz, A., Lemaître, H., …, Greicius, M.D., 2015. Correlated gene expression supports synchronous activity in brain networks. Science 348 (6240), 1241–1244. doi:10.1126/science.1255905.

Ritchie, M.E., Phipson, B., Wu, D., Hu, Y., Law, C.W., Shi, W., Smyth, G.K., 2015. Limma powers differential expression analyses for RNA-sequencing and microarray studies. Nucleic Acids Res. 43 (7), e47. doi:10.1093/nar/gkv007.

Rosenberg, M.D., Finn, E.S., Scheinost, D., Papademetris, X., Shen, X., Constable, R.T., Chun, M.M., 2016. A neuromarker of sustained attention from whole-brain functional connectivity. Nat. Neurosci. 19 (1), 165–171. doi:10.1038/nn.4179.

Salehi, M., Greene, A.S., Karbasi, A., Shen, X., Scheinost, D., Constable, R.T., 2020. There is no single functional atlas even for a single individual: functional parcel definitions change with task. Neuroimage 208, 116366. doi:10.1016/j.neuroimage.2019.116366.

Saygin, Z.M., Osher, D.E., Norton, E.S., Youssoufian, D.A., Beach, S.D., Feather, J., Gaab, N., Gabrieli, J.D.E., Kanwisher, N., 2016. Connectivity precedes function in the development of the visual word form area. Nat. Neurosci. 19 (9), 1250–1255. doi:10.1038/nn.4354.

Scheinost, D., Kwon, S.H., Shen, X., Lacadie, C., Schneider, K.C., Dai, F., Ment, L.R., Constable, R.T., 2016. Preterm birth alters neonatal, functional rich club organization. Brain Struct. Funct. 221 (6), 3211–3222. doi:10.1007/s00429-015-1096-6.

Schuh, A., Makropoulos, A., Robinson, E.C., Cordero-Grande, L., Hughes, E., Hutter, J., Price, A.N., Murgasova, M., Teixeira, R.P.A.G., Tusor, N., Steinweg, J.K., Victor, S., Rutherford, M.A., Hajnal, J.V., Edwards, A.D., & Rueckert, D. (2018). Unbiased construction of a temporally consistent morphological atlas of neonatal brain development. BioRxiv, 251512. 10.1101/251512

Shi, F., Salzwedel, A.P., Lin, W., Gilmore, J.H., Gao, W., 2018. Functional brain parcellations of the infant brain and the associated developmental trends. Cereb. Cortex 28 (4), 1358–1368. doi:10.1093/cercor/bhx062.

Smith, S.M., Fox, P.T., Miller, K.L., Glahn, D.C., Fox, P.M., Mackay, C.E., Filippini, N., Watkins, K.E., Toro, R., Laird, A.R., Beckmann, C.F., 2009. Correspondence of the brain's functional architecture during activation and rest. Proc. Natl. Acad. Sci. 106 (31), 13040–13045. doi:10.1073/pnas.0905267106.

Smyser, C.D., Snyder, A.Z., Neil, J.J., 2011. Functional Connectivity MRI in Infants: exploration of the Functional Organization of the Developing Brain. Neuroimage 56 (3), 1437–1452. doi:10.1016/j.neuroimage.2011.02.073.

Takahashi, E., Folkerth, R.D., Galaburda, A.M., Grant, P.E., 2012. Emerging cerebral connectivity in the human fetal brain: an MR tractography study. Cereb. Cortex 22 (2), 455–464. doi:10.1093/cercor/bhr126.

Thirion, B., Varoquaux, G., Dohmatob, E., Poline, J.B., 2014. Which fMRI clustering gives good brain parcellations? Front. Neurosci. 8. doi:10.3389/fnins.2014.00167.

Thomason, M.E., Dassanayake, M., Shen, S., Katkuri, Y., Alexis, M., Anderson, A., Yeo, L., Mody, S., Hernandez-Andrade, E., Hassan, S., Studholme, C., Jeong, J., Romero, R., 2013. Cross-hemispheric functional connectivity in the human fetal brain. Sci. Transl. Med. 5 (173), 173ra24. doi:10.1126/scitranslmed.3004978.

Turk, E., van den Heuvel, M.I., Benders, M.J., de Heus, R., Franx, A., Manning, J.H., Hect, J.L., Hernandez-Andrade, E., Hassan, S.S., Romero, R., Kahn, R.S., Thomason, M.E., van den Heuvel, M.P., 2019. Functional connectome of the fetal brain. J. Neurosci. 39 (49), 9716–9724. doi:10.1523/JNEUROSCI.2891-18.2019.

van den Heuvel, M.I., Turk, E., Manning, J.H., Hect, J., Hernandez-Andrade, E., Hassan, S.S., Romero, R., van den Heuvel, M.P., Thomason, M.E., 2018. Hubs in the human fetal brain network. Dev. Cognit. Neurosci. 30, 108–115. doi:10.1016/j.dcn.2018.02.001.

van den Heuvel, M.P., Sporns, O., 2019. A cross-disorder connectome landscape of brain dysconnectivity. Nat. Rev. Neurosci. 20 (7), 435–446. doi:10.1038/s41583-019-0177-6.

Vinh, N.X., Epps, J., Bailey, J., 2009. Information theoretic measures for clusterings comparison: is a correction for chance necessary? In: Proceedings of the 26th Annual International Conference on Machine Learning, pp. 1073–1080. doi:10.1145/1553374.1553511.

Wang, D., Buckner, R.L., Fox, M.D., Holt, D.J., Holmes, A.J., Stoecklein, S., Langs, G., Pan, R., Qian, T., Li, K., Baker, J.T., Stufflebeam, S.M., Wang, K., Wang, X., Hong, B., Liu, H., 2015. Parcellating cortical functional networks in individuals. Nat. Neurosci. 18 (12), 1853–1860. doi:10.1038/nn.4164.

Yeo, B.T., Krienen, F.M., Chee, M.W., Buckner, R.L., 2014. Estimates of segregation and overlap of functional connectivity networks in the human cerebral cortex. Neuroimage 88, 212–227. doi:10.1016/j.neuroimage.2013.10.046.

Yeo, B.T., Krienen, F.M., Sepulcre, J., Sabuncu, M.R., Lashkari, D., Hollinshead, M., Roffman, J.L., Smoller, J.W., Zöllei, L., Polimeni, J.R., Fischl, B., Liu, H., Buckner, R.L., 2011. The organization of the human cerebral cortex estimated by intrinsic functional connectivity. J. Neurophysiol. 106 (3), 1125–1165. doi:10.1152/jn.00338.2011.

Yu, X., Ferradal, S., Sliva, D.D., Dunstan, J., Carruthers, C., Sanfilippo, J., Zuk, J., Zöllei, L., Boyd, E., Gagoski, B., Grant, P.E., & Gaab, N. (2020). Infant functional connectivity fingerprints predict long-term language and pre-literacy outcomes. BioRxiv, 2020.10.29.360081. 10.1101/2020.10.29.360081